Journal of Engineering Science and Technology
Vol. 17, No. 6 (2022) 4130 - 4143

AN AMALGAMATION OF ACTIVE APPEARANCE MODEL AND OPPONENT COLOR LOCAL BINARY PATTERN IN AGE ESTIMATION

QUAN-YAN CHANG, SIEW-CHIN CHONG*, THIAN-SONG ONG

Faculty of Information Science and Technology,
Multimedia University, Jalan Ayer Keroh Lama, 75450 Melaka, Malaysia
*Corresponding Author: chong.siew.chin@mmu.edu.my

Abstract

Facial images are broadly used in differentiating various types of personality traits including age recognition. Age estimation is used to determine a person's age based on their biometric feature characteristics. In this proposed work, age estimation is evaluated by extracting the important features of the facial appearance. This paper presents two ways of age estimation implementations, namely Two-Step Implementation and Score-Level Implementation by utilizing the methods of Active Appearance Model (AAM) and Opponents-Color Local Binary Pattern (OCLBP). In both implementations, the weaknesses of AAM and OCLBP are minimized and the strengths of both are used to complement each other for a better age estimation model. The benchmarked age estimation datasets have been used to evaluate the proposed implementation method with promising results generated.

Keywords: Active appearance model, Age estimation, Face recognition Local binary.

1. Introduction

Biometrics can be used to identify individual in the group for public surveillance and monitoring. Facial and gait recognition are some of such useful biometric modalities. In this context, face biometrics has been considered to be the most natural of all biometric measurements. It is easy to implement and well accepted by public. Yet, no physical interaction is required by the user. Thus, it would be more suitable for age estimation in real-world application.

Recently the interest in utilizing face images to estimate age has significantly increased, due to the popularity of computer vision to predict a human's age in real-time applications such as security clearance, age limited vending machine and smart advertising board with dynamic contents.

Face images can be used to enhance the speed of processing in age estimation if compared to gait patterns. However, there are still some limitations of using face images for age estimation.

Most of the problems are related to accuracy performance in estimating age, such that some of the algorithms require huge computation time to achieve precise accuracy, and this might not be practical to real world applications. In fact, there are some well-designed existing methods such as AAM and OCLBP, which could be further enhanced to extend their limitations.

In view of this motivation, our proposed work with Two-Step Implementation and Score-Level Implementation can assist to perform better in estimation of a person's age, which will be deliberated in the section 2 of related works.

2.Related Works

Over the years more and more researchers are growing interest in age estimation area. There are a lot of works being published in this area, with the intention to solve the age estimation problems. Literally, there are several types of age aging models as explained in the following sub-sections.

2.1. Anthropometric model

Among a few popular age estimation methods in Anthropometric model, the work of [1] examines the wrinkles to categorize between young and senior adults. However, it is limited to categorize minors from adult groups, but it is not designed for classification based on different adult age groups. Furthermore, it is sensitive to head pose without involving head texture information.

Later, a method [2] of detecting 10 anthropometric facial fiducial point was introduced. Each point is associated with discriminatory anthropometric features. An efficient feature extraction method was proposed by [3] based on fast independent component analysis (Fast ICA). The distance metric is also learned by using Kande-Lucas-Tomasi (KLT). In their experiments, Mean Absolute Error (MAE) is reduced significantly when the hybrid feature extraction is used.

Recently, Alessio et al. [4] utilized the face shape parameters in their predictive model to predict the body shape parameters using anthropometric measurements.

2.2. Active appearance model

Another prominent age estimation method as proposed in literature is Active Appearance Model (AAM) [5]. It aims to extricate the appearance features to describe the texture and shape of an object with a set of parameters under various physical and environmental circumstances. Besides, another researcher [6] proposed an enhanced version of AAM which is termed as Adaptive Active Appearance model (AAAM). AAAM addresses the challenges to fit a gradient matrix of AAM to video content sequences due to different video qualities. In recent year, a supervised appearance model, sAM [7] has improved AAM using partial least-square regression to replace principle component analysis (PCA), due to the fact that the PCA dimensionality is not considered on the predicted variable related to the classification label. Wrinkle Oriented Active Appearance Model (WOAAM) [8] proposed a new way by integrating distribution of wrinkles into AAM to approximate an empiric joint probability density.

2.3. Aging pattern subspace

Under this category, the authors [9] proposed Aging Pattern Subspace (AGES) to trace the aging pattern using the time order sequence of face images in a representative linear subspace. Two stages namely learning stage and age estimation stage are involved. In the learning stage, the main process is to construct a representative subspace of aging pattern. For the age estimation stage, it uses a single test face images to find out the most suitable age using the position of image sequences. Lately, label distribution learning [10] was used in estimating facial age. By swapping an instance's single label for label distribution, the learning of multiple classes can be made by one instance. Their method shows the benefits of absorbing the correlated classes through learning.

2.4. Age manifold model

ODLPP [11] is one of the Age Manifold Models. The method focuses on orthogonal face recognition to search for discriminant locality preserving projections. Conformal Embedding Analysis [12] demonstrates the high dimensional data projection onto the unit hypersphere with local graph modelling. Meanwhile, the intrinsic neighbour relations are preserved. Another Age Manifold Model named Locally Adjusted Robust Regressor [13] is designed to extract face aging features for learning and estimating human ages. The Pose Data Space [14] which is considered as a union of submanifolds can be used to characterize different subjects. This manifold embedding algorithm dually supervised by both identity and pose information.

2.5. Appearance features model

The work in [15] models Appearance Features Model by dividing the input images into small regions. The method is able to classify the younger and older facial images according to their ages with 10 years intervals. Another variation of Linear Discriminant Analysis (LDA) was introduced in [16] to deal with intrinsic age ambiguity problem by defining age membership functions. It extracts the features by using Gabor filter with LDA classifiers to work out the coarse age classification.

2.6. Other age estimation models

Lately, deep learning has been actively involved in various sectors of image processing including age estimation. Divide-and-Rule Strategy and neural network [17] have been introduced to estimate human age. Recently, age-oriented regression [18] improves the result by utilizing the Relevant Component Analysis (RCA) for distance adjustment and dimension reduction. It trains the connection between features and age label. Besides, deep learning technique using convolutional neural network (CNN) [19] was proposed in the age estimation. Manifold learning algorithm is adopted and shows the robustness of discriminative subspace learning of the deep learned pattern. The opponent colour Local Binary Pattern (OCLBP) [20] in practice increases the large illumination variation whereas the original Local Binary Pattern decreases the lighting effects, which involves the complex local interactions. The OCLBP descriptor performs better through RGB colour if compared to other colour texture descriptors.

3. Proposed Solution

With respect to the problems discussed in the previous sections, Two-Stage Implementation, namely CAAM and Score-Level Implementation, dubbed C+AAM are proposed to take the advantage of both Active Appearance Model (AAM) and Opponents-Color Local Binary Pattern (OCLBP) [20] in extracting face features and in eliciting the useful information for a reliable facial age estimation task. The overall process of two implementations proposed in this paper is shown in Fig. 1.

Motivated by the existing problems in the age-aging model to enhance the performance of age estimation, the proposed method is designed to iron out the weaknesses while absorb the advantages of these methods. Specifically, we adopt Active Appearance Model (AAM) to jointly extract the shape and texture variation from human faces in estimating aging patterns. However, the age label might not be accurately reflected by AAM including different personalities, poses, expressions and living environment other than ages.

Hence, this limitation can be superseded through OCLBP in the proposed implementation. Unlike conventional grey scale-based Local Binary Pattern (LBP), OCLBP is the enhanced version of the LBP to include the colour information of the facial image. OCLBP tends to produce high dimensional features vector which will cause overhead to the computational time. This eventually can be addressed by dimension reduction using Principle Components Analysis (PCA) to ensure computational efficiency while maintaining the performance accuracy. In short, the highlight of the proposed implementation is to extract the intrinsic shape and texture variation from human faces with a low dimensional efficiently without overburden the training process.

3.1. Two-step implementation: CAAM

CAAM is the solution based on Two-Step Implementation. It uses AAM to extract the facial feature and passes the extracted features to OCLBP.

Firstly, AAM feature is extracted from the original image. In the proposed CAAM, the major facial features are outlined, and the major positions of the face are marked with points as shown in Fig. 2(a).

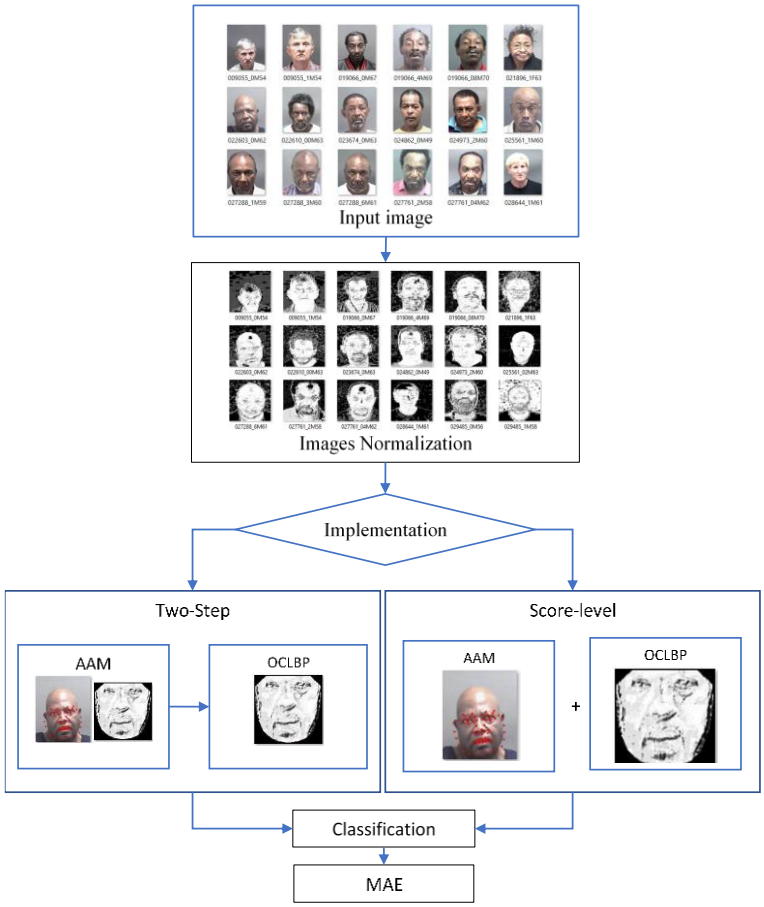

Fig. 1. Overall process of two-step and score-level implementations.

The marked points of an image depict the feature's shape of the image. This is followed by aligning into a co-ordinate frame with the sets, by using vector, v. After that, in order to minimize the dimension of the face features, PCA is then applied to the image with the following approximation:

$$\boldsymbol{v} = \bar{v} + P_v b_v \tag{1}$$

With $\bar{v}$ as the mean shape, P_v represents a set of different variation of orthogonal modes and b_v represents a set of shape parameters. It is necessary to wrap every image to build statistical model of the grey-level appearance, for ensuring the control points can match the mean shape through a triangulation algorithm. By applying the scaling, α and offset, β as well as g_{img} is the reduced features after PCA extraction, the global lighting effect variation is minimized, as shown in Fig. 2(b). Equation (2) formulates the normalized samples, where α and β are best used to match the vector to the normalized mean.

$$g = (g_{img} - \beta 1)/\alpha \tag{2}$$

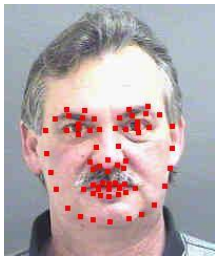

Fig. 2(a). Facial image with landmark point.

Fig. 2(b)1. After cropping and normalizing.

The mean of normalized data, scale and offset is calculated as $\bar{g}$ to produce zero for sum of elements and unity for the variance of the elements. To normalize g_{img} the value of α and β is calculated as below:

$$\alpha = g_{img}.\bar{g}\,, \beta = \left(g_{img}.1\right)/n \tag{3}$$

where n is the number of elements in the vectors.

It is a recursive process to obtain the mean of the normalized data due to the normalization is defined in the terms of the mean. Through estimating the mean, aligning the others to it (using Eq. (2) and Eq. (3)), and then re-estimating the mean and iterating, the process will come to a stable solution. With the use of the PCA, Eq. (4) can produce a linear model:

$$g = \bar{g} + P_g b_g \tag{4}$$

given $\bar{g}$ is the mean of the normalized grey-level vector, P_g is a set of orthogonal mode of the variation and b_g is a set of gray-level parameters. Let vector b_g be the shape of any sample and b_v be the appearance of any example, the data is applied to a further PCA since there may be correlations between shape and greyscale. The concatenated vector of each example, m can be generated as below:

$$m = \begin{pmatrix} w_v m_v \\ m_g \end{pmatrix} = \begin{pmatrix} w_v P_v^T (x - \hat{x}) \\ P_g^T (g - \hat{g}) \end{pmatrix} \tag{5}$$

where w_v is a diagonal matrix of weights for each shape parameter, m_v is the shape parameter, m_g is the colour level parameter.

Let **N** be a neighbourhood, **N** = $\{p_0, p_1, \ldots, p_n\}$ where p_0 is the central pixel and n peripheral pixels p_i, $i \in \{1, \ldots, n\}$. To make it simple, the peripheral pixels are assumed to be arranged circularly around the central one, but this restriction is not necessary. Local Binary Patterns uses a unique decimal code in the instance P of N (i.e., a local image patch) as follows:

$$l_{lbp}(p) = \sum_{i=1}^{n} 2^{i-1} \emptyset[g(p_0), g(p_i)] \tag{6}$$

where given $\emptyset\ (x, y)$ is

$$\emptyset\ (x, y) = \begin{cases} 0 & if\ x \leq y \\ 1 & otherwise \end{cases} \tag{7}$$

Equation (7) represents generic functions that converts colour into grey-scale. The resulting feature vector is the dense and order-less statistical distribution over the set of possible codes.

Opponent-Color Local Binary Patterns (OCLBP) is an extension [12] of LBP which includes colour domain by using intra- and inter-channel features. The calculation of the two channels (*j*, *k*) in the Opponent-Color Local Binary Patterns (OCLBP) is illustrated by the following equation:

$$Ol_{OCLBP_{j,k}}(p) = \sum_{i=1}^{n} 2^{i-1} \emptyset \left(P_{0,j} P_{i,k}\right) \tag{8}$$

where $P_{i,k}$ shows the intensity of the *i*-th pixel in the *k*-th channel. In the RGB space, the image representation is an integration of the feature vectors generated by $OCLBP_{R,G}$, $OCLBP_{R,B}$, $OCLBP_{G,B}$, $OCLBP_{R,R}$, $OCLBP_{G,G}$, $OCLBP_{B,B}$. In the proposed pipeline, the optimum feature vector is selected instead of integration. This is to shorten the dimension of the feature vector. The final OCLBP feature descriptor can be produced using the Eq. (9) before passing to SVM for classification.

$$f_{CAAM} = Ol_{OCLBP_{j,k}}(m) = \sum_{i=1}^{n} 2^{i-1} \emptyset \left(m_{0,j} m_{i,k}\right) \tag{9}$$

The algorithm of the overall process of CAAM is illustrated in Algorithm 1.

Algorithm 1 CAAM

Input: Vector of every image v, Total number of feature K, Total number of AAM feature n
Output: The CAAM vector $\mathbf{f}_1, \ldots, \mathbf{f}_k$.
Process:
1: Initialize $iter = 1$, $iter\_oclbp = 1$, $img = 1$
2: **repeat**
3: Wrap the images with equation 5
4: $iter = iter + 1$
5: **until** $iter == K$
6: **if** mod (img,200) == 0 **then**
7: Store the features batch into new batch file
8: Insert the feature image name and features in vector format.
9: **end if**
10: **repeat**
11. Calculate f_{CAAM} in equation 9
12. $iter\_oclbp = iter\_oclbp + 1$
13. **until** $iter\_oclbp == n$
14. **Return** $\mathbf{f}_1, \ldots, \mathbf{f}_k$.

3.2. Score-level implementation: C+AAM

The second implementation, Score-Level Implementation is named as C+AAM. In C+AAM, the AAM and OCLBP processes will be carried out in parallel. The process of AAM normalization is the same as elaborated in the Section of Two-Step Implementation. The resulted vector of AAM is stored. The calculation can be retrieved from Eq. (5). On the other hand, OCLBP is applied on the raw images. The extracted features of OCLBP are stored separately from AAM. Next, both features generated separately from OCLBP and AAM are fused together with ccaFuse (Feature fusion) method in which a few hyper-parameters such as input $x1$, input $x2$, input $y1$ and input $y2$ are required for fusion purpose.

Given *c*, is the original vector from the input, and *n* represents the total image number, the vector of OCLBP, l can be generated:

$$l_{OCLBP} = Ol_{OCLBP_{j,k}}(c) = \sum_{i=1}^{n} 2^{i-1} \emptyset \left(c_{0,j} c_{i,k}\right) \quad (10)$$

Given vector m, the vector from AAM in the previous Eq. (5), the fused vector can be generated as follows:

$$f_{C+AAM} = \begin{cases} S_{lx}^{-1} S_{ly} S_{my}^{-1} S_{mx} \widehat{W}_x = A^2 \widehat{W}_x \\ S_{my}^{-1} S_{mx} S_{lx}^{-1} S_{ly} \widehat{W}_y = A^2 \widehat{W}_y \end{cases} \quad (11)$$

where $\widehat{W}_x$ and $\widehat{W}_y$ are the eigenvectors and A^2 is the diagonal matrix of the eigenvalues or squares of the canonical correlations. In each equation, the number of non-zero eigenvalues is $d = rank\ (sxy) <= min(n, p, q)$, and it is arranged in decreasing order, $a_1 \geq a_2 \geq a_3 \geq a_d$. Note that f_{C+AAM} in the Equation 11 is based on the fusion of AAM and OCLBP. SVM will be used for classification on top of the fused features.

The algorithm of the overall process is presented in Algorithm 2.

Algorithm 2 C+AAM

Input: Vector of every image v, Total number of feature K, Total number of AAM feature n
Output: The C+AAM vector $\mathbf{f}_1, \ldots, \mathbf{f}_k$.
Process:
1: Initialize $iter = 1$, $iter\_oclbp = 1$, $img = 1$
2: **repeat**
3: Wrap the images with equation 5
4: $iter = iter + 1$
5: **until** $iter == K$
6: **if** mod (img,200) == 0 **then**
7: Store the features batch into new batch file
8: Insert the feature image name and features in vector format
9: **end if**
10: **repeat**
11. Calculate l_{OCLBP} in equation 10
12. $iter\_oclbp = iter\_oclbp + 1$
13. **until** $iter\_oclbp == n$
14. Fusion OCLBP with AAM using equation 11
15. **Return** $\mathbf{f}_1, \ldots, \mathbf{f}_k$.

4. Aging Datasets

Experiments are carried out based on two popular benchmarked facial aging datasets, namely Face and Gesture Recognition Research Network (FG-NET) [22] and Craniofacial Longitudinal Morphological Face Database (MORPH) [23] to evaluate and analyse the performance of the proposed implementations. Both datasets were developed in uncontrolled and controlled environment, respectively. The datasets compose of different facial variations which can present the real-world scenario. Table 1 shows the details of both datasets.

Table 1. Details of FG-NET and MORPH datasets.

Dataset	FG-NET	MORPH
Age range	0-69	15-68

Subjects	82	631
Total image	1002	1690

FG-NET dataset is built with the facial image and landmarks which consists of new-born to 69 years old. There is an average of 12 pictures for each of the 82 subjects in between 0 to 69 years old, yielding the total of 1002 images with different quality, resolution and viewpoint, image sharpness, illumination and facial expression. Each of the images was manually interpreted with 68 landmarks points. Some sample of facial images of FG-NET Database is listed in Fig. 3. Several images consist of the occlusions of spectacles, accessories such as hats and facial hair.

Meanwhile, MORPH dataset consists of two groups: Album1 and Album2. There are 1690 greyscale images from 631 subjects between 15 and 68 years old in Album1. Every image is tagged with additional information about race, gender, glasses, age and facial hair, while there are 55608 images of 13673 subjects between 16 to 99 years old in Album2. Some sample images of MORPH dataset are shown in Fig. 4.

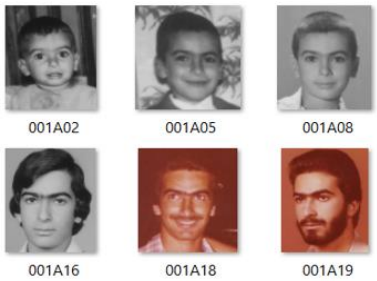

Fig. 3. Sample images of FG-NET dataset [22].

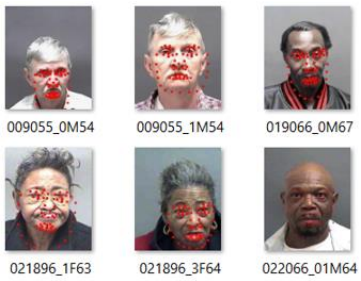

Fig. 4. Sample images of MORPH dataset [23].

5. Proposed Solution

The experimental results are evaluated using the Mean Absolute Error (MAE) based different parameter settings for FG-NET and MORPH datasets. MAE is the mean difference of the real age and the estimated age. The lower score of MAE, the better performance of the age prediction. The formula of MAE is given as follows:

$$MAE = \frac{\sum_{i=0}^{n} |EA_i - RA_i|}{n} \tag{12}$$

In the experiment setup, Leave-One-Person-Out (LOPO) protocol which is similar to the existing works of age estimation, is applied. Experiments are conducted to evaluate the difference of actual age and estimated age respectively, as well as the performance of the training model.

Table 2 summarises the experimental setting of FG-NET and MORPH facial datasets which contains total image of 1002 and 1980 respectively. In MORPH dataset, an average of 4 images per subject are selected where 2 images are used for training and the other 2 images are reserved for testing purposes. For the FG-NET dataset, it is composed of 82 subjects and there are 12 images per subject, whereby there are 6 training images and 6 testing images. In the experiment, the original facial images are cropped into the dimension of 132×133 pixels. The

unwanted background is removed from the images. Normalization is then applied on each image to reduce the background noise from the facial images. The experiment platform is built on 64-bit Operating System with 8GB RAM on fifth Generation Intel Core I7 processor.

Table 2. Experiment settings of FG-NET and MORPH datasets.

Face Dataset	FG-NET	MORPH
Total images	1002	1980
Number of subjects	82	631
Average image per subject	12	4
Total training images per subject	6	2
Total testing images per subject	6	2

All of the experiments are conducted based on various hyper-parameters to evaluate the performance of the proposed solutions. The parameter settings of different processes in the experiment are listed in Table 3.

Table 3. Different parameter settings of various processes.

AAM	SCALES OF THE IMAGES, SCALES	1
	AAM free shape max ($shape\_\max\_x$)	2
OCLBP	filtDims	3×3
	Color channel combine (chnsComb)	[1,1; 2,2; 3,3]
	isEfficent	true
SVM	SVM type	svm_mixed
	SVM Train	true
	SVM Test	true
SVM	Kernel type (kernel_type)	polynomial

Figure 5 shows the overall MAE result of different Neighbours Dimension setting using Channel Combine and Inter Color Relation. The best setting of FG-Net database falls on the Neighbour Dimension of [3,3] with MAE 4.3816 using the Channel Combine method while the lower MAE for MORPH database falls under the Neighbour Dimension [4,4] with MAE 4.4061 using the Color Relation methods. Obviously, the MORPH images captured under controlled environment can perform better than FG-NET images.

In the second implementation, C+AAM, different hyper-parameters are tested as well. Figure 6 shows the comparison of Channel Combine and Color Relation methods of C+AAM using FG-Net and MORPH datasets, where the lowest MAE 4.4174 of FG-Net with the Channel Combine method can be achieved. The optimum setting for MORPH is MAE 4.4192 using the Inter Color Relation method. Neighbour dimension [3,3] performs better in FG-Net with the 4.4174 on Channel Combine method where MORPH performs better in Inter Color Relation with neighbour dimension of [3,3] with the MAE of 4.4192.

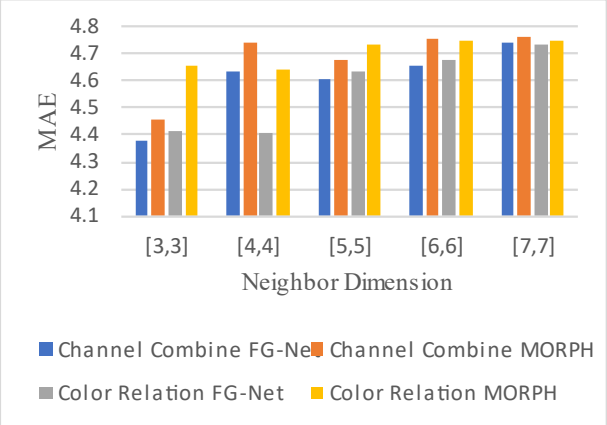

Fig. 5. MAE performance of different neighbor dimension setting using the channel combine and inter color relation in CAAM.

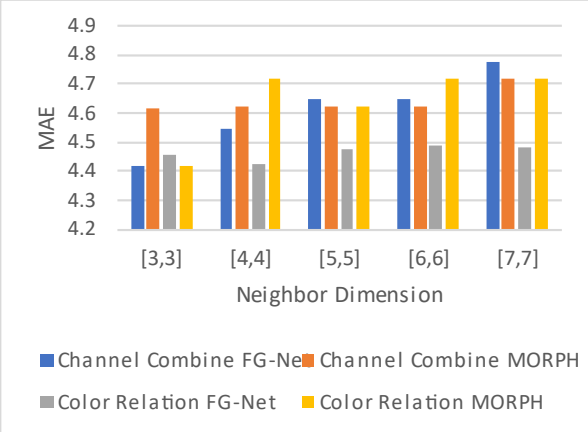

Fig. 6. MAE performance of different neighbor dimension setting using the channel combine and inter color relation in C+AAM.

Cumulative Score also has been computed and compared. Figure 7 illustrates the comparison of cumulative score from FG-Net dataset. CAAM is performing better compared to C+AAM and pure AAM.

As shown in Table 4, CAAM performs better than C+AAM and the rest of the existing works. Here, only the existing works which have similar field of study are compared in the table. In another words, only those existing age estimation methods focused on feature extraction process using facial images with simple implementation are compared. The best result of CAAM can be achieved at MAE 4.4061 using FG-Net after several experiment trials while MAE 4.4555 can be obtained using MORPH. On the other hand, C+AAM generates promising result of MAE 4.4174 using FG-Net while MAE of 4.4192 using MORPH. With the optimistic results obtained, it can be concluded that CAAM is more efficient in extracting useful features than C+AAM. This may be due to extracting in two stages subsequently can minimize the noises of the local feature representation.

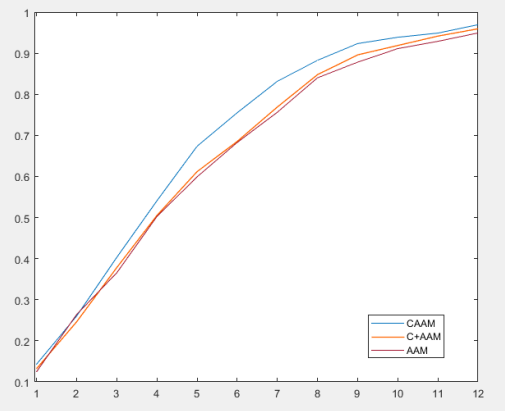

Fig. 7. Cumulative Score of CAAM, C+AAM and AAM from FG-Net dataset.

Table 4. Comparison of proposed implementations and state-of-the-art methods in facial age estimation.

	Methods	FG-NET	MORPH
Proposed	CAAM	4.4061	4.4555
	C+AAM	4.4174	4.4192
State-of-the-art	RUN1 [14]	-	8.34
	SVR [25]	-	5.91
	$AGES_{lda}$ [9]	4.677	6.22
	AAM [25]	4.766	4.72
	CPNN [10]	4.76	4.87
	sAM QF [7]	5.49	-
	HPCA [26]	4.63	-

Table 5 shows the average speed of testing whole set of 1002 images on FG-Net dataset and 1980 images which need only 0.089 to 0.098 seconds for the whole testing process, which proves the computational efficient. Recently, there are various deep learning methods reported actively in age estimation sectors such as [24] which may achieve MAE 2.87 on MORPH and MAE 3.01 on FG-NET. Deep learning methods are known to be an effective method resulted from the massive training on gigantic amount of data. With more and more data for training, the performance continues to increase. However, this might not be a computation friendly solution and might be burden with limited resources in real-world applications. The objective of this paper is to evaluate solely on the computational performance on the simplistic algorithm without relying on exceptionally large number of trainings. Therefore, deep learning methods are not used to compare with the proposed work.

Table 5. Average speed of testing of FG-Net and MORPH datasets.

Methods	Average speed (seconds)	
	FG-Net	MORPH
CAAM	0.089	0.095
C+AAM	0.093	0.098

6. Conclusion and Future Works

In this work, two different implementations in human age estimation through face images are discussed, namely as CAAM and C+AAM. Among these two implementations, the main algorithms involved are AAM and OCLBP. The implementations absorb the strengths of both original algorithms and pleasantly iron the weaknesses of both. The performance has been assessed with two benchmarked datasets which are FG-NET dataset and MORPH dataset, and the promising MAE results are produced compared to the state-of-the-art methods. This proves the efficiency and straightforward implementations of both methods in playing the crucial role in estimating human age. Since deep learning shows its superiority in machine learning, our future work is to adopt the deep learned aging pattern in the proposed formulation to complement the overall performance in term of computational time and accuracy for automatic age estimation.

References

1. Kwon, Y.H.; and da Vitoria Lobo, N. (1999). Age classification from facial images. *Computer Vision and Image Understanding*, 74(1), 1-21.
2. Gupta, S.; Castleman, K.R.; Markey, M.K.; and Bovik, A.C. (2010). Texas 3D face recognition database. *Proceedings of the* 2010 *IEEE Southwest Symposium on Image Analysis & Interpretation* (*SSIAI*), Austin, TX, USA, 97-100.
3. Kumar, S.; Ranjitha, S.; and Suresh, H.N. (2017). An active age estimation of facial image using anthropometric model and fast ICA. *Journal of Engineering Science and Technology Review*, 10(1), 100-106.
4. Gallucci, A.; Znamenskiy, D.; and Petkovic, M. (2020). Prediction of 3D body parts from face shape and anthropometric measurements. *Journal of Image and Graphics*, 8(3), 67-74.
5. Cootes, T.F.; Edwards, G.J.; and Taylor, C.J. (1998). Active appearance models. in *Lecture Notes in Computer Science* (*including subseries Lecture Notes in Artificial Intelligence and Lecture Notes in Bioinformatics*), 484-498.
6. Liu, X. (2010). Video-based face model fitting using adaptive active appearance model. *Image and Vision Computing*, 28(7), 1162-1172.
7. Bukar, A.M.; Ugail, H.; and Connah, D. (2016). Automatic age and gender classification using supervised appearance model. *Journal of Electronic Imaging*, 25(6), 061605.
8. Martin, V.; Séguier, R.; Porcheron, A.; and Morizot, F. (2019). Face aging simulation with a new wrinkle oriented active appearance model. *Multimedia Tools and Applications*, 78: 6309-6327.
9. Geng, X.; Zhou, X.; Zhang, Y.; Li, G.; and Dai, H. (2007). Learning from facial aging patterns for automatic age estimation. *Proceedings of the* 14*th annual ACM international conference on Multimedia*, 307-316.
10. Geng, X.; Yin, C.; and Zhou, Z.-H. (2013). Facial age estimation by learning from label distributions. *IEEE Transactions on Pattern Analysis and Machine Intelligence*, 35(10), 2401-2412.
11. Zhu, L.; and Zhu, S. (2007). Face recognition based on orthogonal discriminant locality preserving projections. *Neurocomputing*, 70(7-9), 1543-1546.

12. Fu, Y.; Liu, M.; and Huang, T.S. (2007). Conformal embedding analysis with local graph modeling on the unit hypersphere. *Proceedings of the IEEE Computer Society Conference on Computer Vision and Pattern Recognition*. Minneapolis, MN, USA, 1-6.
13. Guo, G.; Fu, Y.; Dyer, C.R.; and Huang, T.S. (2008). Image-based human age estimation by manifold learning and locally adjusted robust regression. *IEEE Transactions on Image Processing*, 17(7), 1178-1188.
14. Yan, S.; Wang, H.; Fu, Y.; Yan, J.; Tang, X.; and Huang, T.S. (2009). Synchronized submanifold embedding for person-independent pose estimation and beyond. *IEEE Transactions on Image Processing*, 18(1), 202-210.
15. Gunay, A.; and Nabiyev, V. V. (2008). Automatic age classification with LBP. *Proceedings of the* 2008 23*rd International Symposium on Computer and Information Sciences*, Istanbul, Turkey, 1-4.
16. Gao, F.; and Ai, H. (2009). Face age classification on consumer images with gabor feature and fuzzy LDA method. *Lecture Notes in Computer Science*. 132-141.
17. Liao, H.; Yan, Y.; Dai, W.; and Fan, P. (2018). Age estimation of face images based on CNN and divide-and-rule strategy. *Mathematical Problems in Engineering*, Volume 2018, Article ID 1712686.
18. Chao, W.-L.; Liu, J.-Z.; and Ding, J.-J. (2013). Facial age estimation based on label-sensitive learning and age-oriented regression. *Pattern Recognition*, 46(3), 628-641.
19. Wang, X.; Guo, R.; and Kambhamettu, C. (2015). Deeply-learned feature for age estimation. *Proceedings of the* 2015 *IEEE Winter Conference on Applications of Computer Vision*, Waikoloa, HI, USA, 534-541
20. Chelali, F.Z.; and Djeradi, A. (2015). CSLBP and OCLBP local descriptors for speaker identification from video sequences. *Proceedings of the* 2015 *Third World Conference on Complex Systems* (*WCCS*), Marrakech, Morocco, 1-7.
21. Mäenpää, T.; and Pietikäinen, M. (2005). Texture analysis with local binary patterns. *Handbook of Pattern Recognition and Computer Vision*,197-216.
22. Panis, G.; and Lanitis, A. (2015). An overview of research activities in facial age estimation using the FG-NET aging database. *Lecture Notes in Computer Science*, 737-750.
23. Ricanek, K.; and Tesafaye, T. (2006). MORPH: a longitudinal image database of normal adult age-progression. *Proceedings of the* 7*th International Conference on Automatic Face and Gesture Recognition* (*FGR*06), Southampton, UK, 341-34.
24. Sendik, O.; and Keller, Y. (2019). DeepAge: Deep learning of face-based age estimation. *Signal Processing: Image Communication*, 78, 368-375.
25. Luu, K.; Ricanek, K.; Bui, T.D. and Suen, C.Y. (2009). Age estimation using active appearance models and support vector machine regression. *Proceedings of the* 2009 *IEEE* 3*rd International Conference on Biometrics: Theory, Applications, and Systems*, Washington, DC, USA, 1-5.
26. Sahoo, T.K.; and Banka, H. (2017). New hybrid PCA-based facial age estimation using inter-age group variation-based hierarchical classifier. *Arabian Journal for Science and Engineering*, 42, 3337-3355.